

RSC Advances



This is an *Accepted Manuscript*, which has been through the Royal Society of Chemistry peer review process and has been accepted for publication.

Accepted Manuscripts are published online shortly after acceptance, before technical editing, formatting and proof reading. Using this free service, authors can make their results available to the community, in citable form, before we publish the edited article. This *Accepted Manuscript* will be replaced by the edited, formatted and paginated article as soon as this is available.

You can find more information about *Accepted Manuscripts* in the [Information for Authors](#).

Please note that technical editing may introduce minor changes to the text and/or graphics, which may alter content. The journal's standard [Terms & Conditions](#) and the [Ethical guidelines](#) still apply. In no event shall the Royal Society of Chemistry be held responsible for any errors or omissions in this *Accepted Manuscript* or any consequences arising from the use of any information it contains.

Promoting the cyclic and rate performance of lithium-rich ternary materials via surface modification as well as lattice expansion

Mohammed Adnan Mezaal^{a,b}, Limin Qu^a, Guanghua Li^a, Rui Zhang^a, Jiang Xuejiao^a, Ke Zhang^a, Wei Liu^a and Lixu Lei^{*.a}

^a*School of Chemistry and Chemical Engineering, Southeast University, Nanjing, 211189, People's Republic of China.*

^b*Department of Chemistry, College of Science, University of Karbala, Karbala, 56001, Iraq.*

*Corresponding Author. Tel.: +86-25-52090620-6421, Fax: +86-25-52090618.

E-mail address: lixu.lei@seu.edu.cn

Abstract

Nickel-rich layered lithium transition-metal oxides, $\text{Li}_{1.2}\text{Ni}_{1-x}\text{M}_x\text{O}_2$ (M=transition metal), have been studied intensively as high-energy positive-electrode materials for lithium batteries because of their high specific capacity and relatively low-cost. However, oxygen loss from the lattice during the initial charge and gradual structural transformation during cycling can lead to capacity degradation and potential decay of the cathode materials. This is due to the small size and highly oxidizing nature of tetravalent nickel. Herein, we report for the first time a series of promising core-shell structured positive-electrode materials with a general formula $[\text{Li}_{1.2-x}\text{Na}_x\text{Ni}_{0.62}\text{Co}_{0.14}\text{Mn}_{0.248}\text{O}_2]$, where $x = 0, 0.05, 0.08, 0.10$ and 0.12 . The results clearly show that manganese oxide coating has greatly improved the cycling stability and inhibited the side reactions with the electrolytes. However, manganese oxide coating can also retard the electrode reactions because it extends the diffusion path for lithium

ion and results in increases the charge transfer resistance. Sodium doping expands the lattice due to the fact that Na has higher ionic radii than that of Li. This facilitates the diffusion of Li-ions, reduces the charge transfer resistance and improves the electrochemical performance of the materials. Furthermore, sodium doping not only improves the discharge capacity, but it also improves the cycling stability even further. This is because Na has higher ionic radii than that of Li and hence Na has less tendency to migrate to “tetrahedral” sites in the Li/Na layer and restricts the structural transformation. However, addition of Na higher than 0.1 decreases the capacity as Na has higher weight than that of Li.

Keywords: Nickel-rich materials, manganese oxide; nanoscale coating, sodium doping, charge transfer resistance, lithium diffusion, lithium ion battery

1. Introduction

The world energy consumption and environmental pollution have been increasing exponentially during the last decades, which force us to quest for a green and low-cost energy resources. The green sources of energy such as solar, wind energy and wave are periodic. Therefore, an efficient battery is needed to store the energy in chemical form and convert to electricity when needed. Lithium ion battery system (LIBs) has been regarded as one of the most promising solutions due to its high energy density and long lifespan.¹ Current lithium ion battery technology is well-developed for portable electronic devices, but still need to be improved to fit the requirement for

high-power systems like plug-in hybrid electric vehicles (PHEV) and electric vehicles (EV) in many perspectives, such as energy density, safety, durability and cost.^{2,3}

Among all the positive-electrode materials, LiCoO_2 is the most used and qualified. However, its energy density also fails to meet the demands of today's consumers, it is not stable to heavy duties and very expensive because Co is rare.^{4, 5} Therefore, researches on substitution of Co for cheaper and abundant elements, such as Mn and Ni, have been main concerns in last decades. One of the successful examples is $\text{Li}[\text{Ni}_{1/3}\text{Co}_{1/3}\text{Mn}_{1/3}]\text{O}_2$, which has already been commercialized for auto-mobile applications because it is relatively cheaper than LiCoO_2 and its outstanding safety characteristics. However, its capacity of 155 mAh g^{-1} is quite low to be use in next generation EVs applications.^{6,7}

It has been found that Ni-rich materials (Ni content > 60%) are promising cathode candidates for Li-ion batteries because of their high energy density, and low cost. In addition, they can deliver higher discharge capacities and work at higher voltages (4.4-4.8V)⁸⁻¹⁰ than $\text{Li}[\text{Ni}_{1/3}\text{Co}_{1/3}\text{Mn}_{1/3}]\text{O}_2$, because the higher Ni content makes the main active redox species ($\text{Ni}^{2+} \leftrightarrow \text{Ni}^{4+}$) more in the layered structure. However, fast capacity fading, poor thermal stability still plague their mass application. Furthermore, they can easily transform into an electrochemically inactive NiO-like or spinel phase with high volumetric changes. This is due to the small size and highly oxidizing nature of tetravalent nickel and it can result in the loss of oxygen, and migration of nickel ions to the lithium-depleted layer. The increased formation of NiO phase results in capacity

fading, and moreover, repeated volumetric changes can result in the pulverization of the original active materials. This instability of the delithiated phase also causes safety issues and capacity fading.^{2, 8, 11-16} In addition, cycling the positive-electrode material at a temperature greater than 60 °C can also catalyze the reaction between electrode surface and electrolytes, which forms a non-conducting solid electrolyte interface (SEI) layer that increases the diffusion path of Li⁺ ion and deteriorates the electrochemical performance of the material.¹⁷⁻¹⁹

To date, intensive research has been carried out to improve such structural stability of Ni-rich materials via surface coating or core shell structuring.^{10, 17, 20-27} Sun *et al* reported a Ni-rich core-shell structured Li[(Ni_{0.8}Co_{0.1}Mn_{0.1})_{0.8}(Ni_{0.5}Mn_{0.5})_{0.2}]O₂, which delivers 200 mAh g⁻¹ at 40 mA g⁻¹ and it delivers a discharge capacity of 120 mA g⁻¹ at 1 C and retains a discharge capacity of 98% after 500 cycles. They have attributed the high capacity to the core Li[Ni_{0.8}Co_{0.1}Mn_{0.1}]O₂) and the good thermal stability to the manganese rich-shell (Li[Ni_{0.5}Mn_{0.5}]O₂ shell).¹¹ Recently, Cho *et al* have synthesized a Ni-rich positive-electrode material LiNi_{0.6}Co_{0.2}Mn_{0.2}O₂ coated with SiO₂ layer, their result showed that its cycle performance and thermal stability can be improved because SiO₂ has reduced the side reaction between the electrode and electrolyte, although the discharge capacity of the material decrease along with increase of Si content due to sluggish kinetics of Li⁺ diffusion.²⁸ Lu *et al* reported a LiMO₂ material coated with nanoscale Li₂TiO₃. They found that the thin film of Li₂TiO₃ has significantly improved the cyclic stability of the material, and the charge transfer resistance of the coated material is much smaller than the uncoated one after many cycles.²⁰ However, all the

materials reported above (Reference^{11, 20}) were cycled at relatively low upper voltage of 4.3 V.

Although considerable research has been done to improve the electrochemical performance of nickel rich materials, it is still need further efforts to design and prepare a more stable nickel rich materials for LIBs. On the other hand, among the positive electrode candidates currently being studied, Li-rich layered oxides are the most attractive for next generation LIBs due to their high specific capacities exceeding 200 mAh g⁻¹.²⁹⁻³²

Sun *et al* reported (Li_{1.2}Ni_{0.62}Co_{0.15}Mn_{0.25}O₂) positive-electrode materials. Their results showed that this material has poor cycling stability and low thermal stability. They also reported that increasing Mn content in the shell can improve the thermal stability of the material.³³ Therefore, in this study, we have chosen the Li-excess Ni-rich materials system (Li_{1.2}Ni_{0.62}Co_{0.14}Mn_{0.24}O₂) to further enhance its stability and to improve its electrochemical performance via manganese coating well as sodium doping, because as reported earlier that manganese coating can provide good thermal stability to the material, while sodium doping can increase the discharge capacity.^{11, 34-36} Our results show that coating the material has significantly improved its cycling stability. However, by using the impedance spectroscopy techniques, we have found that coating the material has increased the charge transfer resistance due to increases of the diffusion path of Li-ions. It has been reported that sodium doping can enlarges the lattices volume, reduces the charge transfer resistance and increases the discharge capacity of layered

structure materials.^{35, 37, 38} Therefore, we have doped the surface modified materials with sodium to reduce its charge transfer resistance and to further improve its electrochemical performance. Na has higher ionic radii than that of Li and because of this fact, Na has expanded the lattice, reduced the charge transfer resistance and significantly increased the discharge capacity of the surface modified materials.

Experimental section

1.1 Syntheses of the materials

All chemicals and reagents used were analytical grade without any further purification. $\text{Ni}_{0.62}\text{Co}_{0.14}\text{Mn}_{0.24}\text{CO}_3$ was synthesized by a typical co-precipitation. Stoichiometric amounts of $\text{NiSO}_4 \cdot 6\text{H}_2\text{O}$, $\text{CoSO}_4 \cdot 7\text{H}_2\text{O}$ and $\text{MnSO}_4 \cdot \text{H}_2\text{O}$ were dissolved in deionized water to prepare 1 M solution, which was added into a 2 M Na_2CO_3 solution in a continuously stirring tank reactor to form a suspension. It had been then aged for 24 h under N_2 atmosphere, during which the temperature and pH value of the solution were precisely controlled at 60 °C and 8.5, respectively. The solid was filtered, washed and dried in a vacuum at 100 °C.

Coating of manganese oxide on the surface of $\text{Ni}_{0.62}\text{Co}_{0.14}\text{Mn}_{0.24}\text{CO}_3$ was achieved as followed: 0.177 g of $\text{MnSO}_4 \cdot \text{H}_2\text{O}$ was dissolved in 50 ml of deionized water and added into 100 ml of aqueous suspension containing 2 g of the precursor $\text{Ni}_{0.62}\text{Co}_{0.14}\text{Mn}_{0.24}\text{CO}_3$ and 0.223 g of Na_2CO_3 . The resulted suspension was aged for 12 h at 60 °C, filtered, washed three times with deionized water and dried in a vacuum at 100 °C.

The final lithiated positive-electrode materials $\text{Li}_{1.2-x}\text{Na}_x\text{Ni}_{0.62}\text{Co}_{0.14}\text{Mn}_{0.248}\text{O}_2$ ($x = 0, 0.05, 0.08, 0.10$ and 0.12) were obtained by mixing stoichiometric powder of the coated precursor with a proper amount of Li_2CO_3 and Na_2CO_3 . The mixture was first heated at $450\text{ }^\circ\text{C}$ for 8 h, followed by baking at $850\text{ }^\circ\text{C}$ for 12 h in air. The furnace ramp rate was maintained at $2\text{ }^\circ\text{C min}^{-1}$. The coated material with the nominal formula $[\text{Li}_{1.2-x}\text{Na}_x\text{Ni}_{0.62}\text{Co}_{0.14}\text{Mn}_{0.248}\text{O}_2]$, where $x = 0, 0.05, 0.08, 0.1$ and 0.12 , have been denoted as S1, S2, S3, S4 and S5, respectively.

The material $\text{Li}_{1.2}\text{Ni}_{0.62}\text{Co}_{0.14}\text{Mn}_{0.24}\text{O}_2$ without coating, denoted as S0, was synthesized with a similar method, except that the uncoated precursor is mixed with a proper amount of Li_2CO_3 directly.

1.2 Physical characterization

Powder X-ray diffraction was performed on a SHIMADZU XD-3A diffractometer in transmission mode with Cu K_α radiation. XRD data was collected at a scan rate of $0.15\text{ }^\circ 2\theta\text{ min}^{-1}$ with 0.02 ° step size in the 2θ range between 10 ° and 80 ° .

The morphology of the materials was observed using a scanning electron microscope (SEM, FESEM Hitachi SU8010). Transmission electron microscopy (TEM) was performed on a JEM2000EX transmission electron microscope. Chemical compositions of the samples were determined using inductively coupled plasma (ICP-OES, Optima 8000).

To test the electrochemical performance, powder samples were mixed with

acetylene carbon black (AB) and poly(vinylidene fluoride) (PVDF), to a weight ratio of 80 : 10 : 10, then dispersed in 1-methyl-2-pyrrolidinone (NMP). The slurry was spread onto a piece of aluminum foil, a typical loading of the thin electrodes is about 2-3 mg cm⁻² and then dried in vacuum oven at 100 °C for 24 h. The test CR 2032 coin cells were assembled in an Ar-filled glove box with Li metal as the counter electrode, 1 M LiPF₆ dissolved in ethylene carbonate (EC) and dimethyl carbonate (DMC) as the electrolyte. The cells were galvanostatically charged/discharged within the range of 2.5 ~ 4.8 V at room temperature instead of upper voltage of 4.5V. The cells were galvanostatically charged at different current densities to 4.8V, followed by additional constant-voltage (CV) charging step at 4.8 V for 20 min and then discharged galvanostatically at the same current density as the charging process to 2.5V using a battery cycler (Land battery testing system) at room temperature. The current densities used were 27, 136, 273, 546, 1092 and 2184 mA g⁻¹, corresponding to C rates, 0.1, 0.5, 1, 2, 4 and 8 C (1 C = 273 mA g⁻¹). Cyclic voltammetry (CV) tests were performed on a CHI660D electrochemical workstation at a sweep rate of 0.5 mV s⁻¹. The electrochemical impedance spectroscopy (EIS) was carried out on an electrochemical analyzer within a frequency range between 10⁵ Hz ~0.01 Hz and an AC amplitude of 5 mV.

2. Results and discussion

2.1 Structure and morphology

The elemental analyses of the samples were performed using the ICP-OES

technique. The results are shown in Table 1, which demonstrate that the observed values are approximately consistent with the proposed ones. The observed values of manganese are slightly higher than the proposed values because manganese ions has lower solubility than both of nickel and cobalt ions at the PH of the reaction.

The XRD patterns in Figure 1 show that the synthesized samples are all phase-pure without any impurity peaks detected. All the diffraction peaks of the XRD pattern could be indexed based on the layered hexagonal structure of α -NaFeO₂ type lattice belonging to the space group $R\bar{3}m$.³⁹⁻⁴² There is no reflection appears in the ~ 20 – 23° 2θ range that indicates the absence of Li₂MnO₃ phase due to the low content of manganese, and the patterns can be described inarguably as a single phase LiMO₂ (see reference⁴³ for more information).^{43, 44} In the XRD patterns, the (006)/(102) peaks of sample S4 are well spilt, suggesting a well-defined layered structure formed in the lattice. A careful analysis of the XRD pattern indicates that the (003) peak of the Na-doped samples move slightly toward the lower angle region. This suggests that the Na ions could be completely introduced into the alkali ion layer in the lattice, which enlarges substantially the Li slab space.³⁸ The lattice parameters and particle sizes are shown in Table 2. The carefully refined lattice parameters indicate that there is no lattice expansion as a result of manganese coating. It can be seen that sodium doping increases the values of a , c and I_{003}/I_{104} due to the fact that Na has higher ionic radii than Li. This lattice expansion can makes the lithium intercalation/de-intercalation easier as well as decreases the degree of cation mixing, which make well-defined layered structure⁴⁵.

Figure 2 shows the SEM images of the samples. The grains of the pristine sample S0 are irregular with dimensions ranging from 300 nm to 500 nm. However, it is less aggregated than the manganese coated sample S1. The grains of the sodium doped samples are secluded from each other and has better crystallinity than the undoped samples. These results indicate that sodium doping significantly improves the crystallinity of the material. The structure and morphology of the rod-like particles appearing in all of the sodium doped samples. They have the same α -NaFeO₂ type structure (space group $R\bar{3}m$) as shown in Figure 3, but they are impurity particles coming from the crucible.

The structure and morphology of the pristine sample S0 and the surface modified material S4 were further characterized by Transmission Electron Microscope (TEM), which is shown in Figure 4. The irregular primary particle of the pristine material is well-crystallized, and its selected area electron diffraction (SAED) pattern exhibits sets of lattice fringes with 0.470 nm, 0.245 nm, 0.237 nm, 0.235 nm, and 0.200 nm interplanar spacing, which corresponds to the (003), (101), (006), (012), and (104) diffractions of the layered structure (α -NaFeO₂ type, space group $R\bar{3}m$), respectively.⁴⁶ Spinel phase in the pristine samples were observed in TEM diffraction pattern, but it could not be observed in the XRD pattern due to the low content of the spinel phase.

The high-resolution transmission electron microscope (HRTEM) image of sodium doped material S4 shows well-crystallized particles and a very uniform shell of ~2.4 nm thickness. The SAED pattern of the sample S4 exhibits a lattice fringe of 0.142 nm,

which can be indexed to the (110) diffraction of the α -NaFeO₂ type structure (space group R $\bar{3}m$). As shown in the enlarged image, the inner part shows a typical layered structure with interplanar spacing of 0.47 nm which corresponds to spacing of (003) planes. These results are in good agreement with the XRD patterns.

Scanning transmission electron microscopy was used to characterize the nanoscale coat on sample S4, Li_{1.09}Na_{0.098}Ni_{0.62}Co_{0.155}Mn_{0.322}O₂ (Figure 5). It can be seen that the intensities of Mn and Li in the shell are much higher than those of Ni and cobalt. This indicates that the outer layer was manganese oxide, but it was lithiated by Li₂CO₃ at high temperature. The shell thickness is about 2.5 nm which is in good agreement with the previous TEM results. Moreover, Ni, Co and Mn are homogeneously distributed in the core of the particles, as reflected by the EDS line scan results.

2.2 Electrochemical performance

Figure 6a displays the initial charge-discharge curves of the samples at 27 mA g⁻¹ (0.1 C, 1 C = 273 mA g⁻¹). The coated sample S1 delivers a discharge capacity a little lower than the pristine material S0 because the coating of the material even at nanoscale makes the diffusion path of the Li-ions longer which leads to sluggish rate of Li insertion/deintercalation and increases of the charge transfer resistance (Table 3) (see the impedance spectroscopy part in this paper for more information). Sodium doping significantly increases the discharge capacity because sodium doping enlarges substantially the Li slab space and reduces the charge transfer resistance. The Sample S4 shows a flatter discharge platform and it delivers the highest discharge capacity of 265 mAh g⁻¹ at 27mA g⁻¹ among all of the samples. As shown in the enlarged image

(Figure 6a), the discharge curves of the sodium doped samples and especially sample S4 are at higher voltage than the discharge curves of the undoped samples. However, sample S5 delivers less discharge capacity than both of S4 and S3 due to the fact that addition of Na higher than 0.1 decreases the capacity as Na is higher weight than that of Li.

To evaluate the effect of Mn coating and sodium doping on the stability of the materials, samples S0, S1 and S4 have been cycled between 2.0 and 4.8 V at 546 mA g⁻¹. The pristine material S0 delivers a discharge capacity of 175 mAh g⁻¹ initially and its capacity retention is only 74% after 100 cycles (Figure 6b), while the discharge capacity of the Mn-coated sample S1 is 215 mAh g⁻¹ and retains 92% of its capacity after 100 cycles. This results clearly indicates the manganese coated layer is very effective to inhibit the side reactions with the electrolytes.

As can be seen in figure 6b, the sample S4 delivers a discharge capacity of 228 mAh g⁻¹ and retains 95% of its capacity after 100 cycles. This indicates that sodium doping not only increases the discharge capacity, but it does further improves the cycling stability due to the fact that Na has higher ionic radii than Li and because of that Na has less tendency to migrate to “tetrahedral” sites in the Li/Na layer and restricts the structural transformation.

To further study the effect of Na doping and manganese coating on the cycling stability, the cells were cycled between 2.0 and 4.8 V at current densities of 27, 136, 273, 546, 1092 and 2184 mA g⁻¹ at room temperature (Figure 6c). It can be seen that

the pristine sample S0 delivers a discharge capacity of 245 mAh g⁻¹ at 0.1 C, which falls to 104 mAh g⁻¹ at 8 C and 201 mAh g⁻¹ at 0.1 C after overall 37 cycles, which is 84% of the initial value, while those for Mn-coated S1 are 244 mAh g⁻¹ at 0.1 C, 144 mAh g⁻¹ at 8 C and 239 mAh g⁻¹ at 0.1 C at the 100th cycle, which is 97% of the initial value. Such a large capacity fading of the pristine sample could be attributed to the high reactivity of Ni⁴⁺ and Co³⁺ at high voltage toward the electrolytes, which results in the loss of oxygen, migration of the transition metal ions into the lithium-depleted layer, and subsequent degradation of the active material.¹⁴⁻¹⁷ In a comparison with the recently reported LiMO₂ in ref.³³, the coated sample S1 in this work exhibits much improved cycling performance under higher current density.

Sodium doping has increased the discharge capacity remarkably (Figure 6c) at all rates. Among the four sodium-doped samples, S4 delivers the highest discharge capacity at all the rates (Figure 6c). Such excellent rate capability of the Na-doped samples could be attributed to the enlargement of the Li slab space by the Na doping that facilitates the diffusion of lithium ion in the bulk of the material and to the orientation growth of the Na-doped lattice along the direction of the layer, which promotes the fast insertion and extraction of Li ions. It is noteworthy that when the current is reduced back to 0.1 C, the discharge capacity of the S4 cell can recover to 257 mA h g⁻¹ while the pristine cell delivers only 201 mA h g⁻¹. Furthermore, it is found that the discharge capacity increases along with the increase of I_{003}/I_{104} values (Table2) as evaluated from the XRD data. These indicate that sodium doped samples can tolerate the impact of high current density and restrict the structure transformation which result

in an increase in the utilization of the materials.^{35, 37, 38}

Cyclic voltammetry measurements have also been carried out to evaluate the effects of surface modification and sodium doping (Figure 7). The fresh electrode was scanned anodically (Li extraction), followed by a corresponding cathodic scan (Li insertion). One pair of redox peaks was observed for all the prepared samples. It is known that the anodic peaks located in the potential range between 4 and 4.2 V are due to the oxidation process of Ni²⁺ and Co⁺³ to higher oxidation states.⁴⁷ Moreover, sample S0 shows a pair of a broad redox peaks with high potential difference (ΔE_p), which indicates that the redox reaction is hard to take place reversibly. In addition, the anodic peak current of sample S0 is very small in comparison with the others, which indicates a slower rate of the redox reaction. All the surface modified materials show sharper redox peaks, and smaller ΔE_p than the pristine material S0, and the peaks of sodium doped samples are even sharper. Moreover, the anodic peaks of all surface modified materials are at lower potentials than the pristine material, which means that the polarization is reduced. Among all the samples, the anodic peak intensity of sample S4 is the highest, which means S4 components are very easy to be oxidized.

Figure 8 shows the electrochemical impedance spectroscopy (EIS) of the materials after the first cycle, which shows that the charge transfer resistance (R_{ct}) of the surface modified material is higher than that of the pristine material (Table 3). This means that Mn-coating has increased the diffusion path of Li⁺ ion. However, sodium doping has significantly decreased the R_{ct} values, and sample S4 has the smallest R_{ct} value among

all the synthesized samples, which is in accordance with its superior electrochemical performance. This is due to the fact that sodium has a higher ionic radii than Li which expands the lattice C. To further evaluate the structure stability, we have also measured the electrochemical impedance spectroscopy after cycling the cells for 100 times at 2 C (Table 3 and the inset of Figure 8). It is clear that the R_{ct} value of sample S0 increases from 124.9 to 560.8 Ω , but those of the Mn oxide coated samples did not change significantly. This phenomenon has also been found in the literature.²⁸ Therefore, manganese coating has significantly inhibited the growth of SEI film on the surface of the electrode material, as it is well known that the SEI film thickens upon cycling due to the high reactivity of nickel and cobalt ions toward the electrolyte and results in deterioration of the electrochemical performance.²³

The XRD pattern of the synthesized sample S4 after 100 charge-discharge cycles shows that the material is still single phase without any impurity peaks detected (Figure 1-S4'). All the diffraction peaks of the XRD pattern could be indexed based on the layered hexagonal structure of α -NaFeO₂ type lattice belonging to the space group $R\bar{3}m$.³⁹⁻⁴² The calculated a and c values of the cycled material are 2.893 and 14.315, respectively, which are very slightly smaller to the corresponding values of the original material. The 003 peak of the cycled material is a little broader with lower intensity than the original material's peak, which means that the crystallinity of the material is reduced upon cycling. These results indicate that the synthesized material is very stable even when it cycled at high potential of 4.8 V.

To further evaluate the structure stability of the material, we have characterized

the material after being cycled for 100 charge-discharge cycles by the high-resolution transmission electron microscope (HRTEM) (Figure 9). The SAED pattern exhibits a lattice fringes of 0.47, 0.235, 0.243, 0.186 and 0.143 nm, which can be indexed to the 003, 006, 101, 015 and 018 diffractions of the α -NaFeO₂ type structure, respectively (space group $R\bar{3}m$). As shown in the enlarged image, the inner part shows a typical layered structure with interplanar spacing of 0.47 nm which corresponds to spacing of (003) planes. These results are in good agreement with the XRD pattern. Therefore, the outer Li-Mn-O layer of the particle (shell) has significantly improved the stability of the structure, the material still exhibits single phase and there is little structural changes observed after 100 charge-discharge cycles.

Conclusions

In summary, a series of MnO₂-coated materials [Li_{1.2-x}Na_xNi_{0.62}Co_{0.14}Mn_{0.248}O₂] ($x = 0, 0.05, 0.08, 0.10$ and 0.12) have been successfully synthesized by homogeneous coprecipitation and subsequent calcinations, and the coating layer is 2 ~ 3 nm in thickness.

All the synthesized materials are single phased and isostructural with LiNiO₂ (α -NaFeO₂ type, space group $R\bar{3}m$). The coating layer increases the diffusion path of lithium ion and increases the charge transfer resistance (R_{ct}). However, it has significantly improved the cycling stability even when the material cycled at high voltage of 4.8V and high current density.

A proper amount of sodium doping has improved the crystallinity of the material, substantially expanded the Li slab space due to the higher ionic radii of Na than that of Li which resulted in reduced R_{ct} value and improved the discharge capacity. Furthermore, Sodium has improved the cycling stability even further due to the fact that Na has higher ionic radii than that of Li and because of this fact, Na has less tendency to migrate to “tetrahedral” sites in the Li/Na layer and restricts the structural transformation. However, addition of Na higher than 0.1 decreases the capacity as Na is higher weight than that of Li.

ACKNOWLEDGMENTS

This work was supported by the Department of Science and Technology, Jiangsu Province (BY2013073-03), Jiangsu key laboratory for advanced metallic materials (BM2007204), and Analytical Test Fund of Southeast University (201226).

References

1. J. Q. Zhao and Y. Wang, *Journal of Materials Chemistry A*, 2014, **2**, 14947.
2. X. Yang, D. Wang, R. Yu, Y. Bai, H. Shu, L. Ge, H. Guo, Q. Wei, L. Liu and X. Wang, *Journal of Materials Chemistry A*, 2014, **2**, 3899.
3. T.-F. Yi, S.-Y. Yang and Y. Xie, *J. Mater. Chem. A*, 2015, **3**, 5750-5777.
4. R. Santhanam and B. Rambabu, *Journal of Power Sources*, 2010, **195**, 5442-5451.
5. S. Han, Y. Xia, Z. Wei, B. Qiu, L. Pan, Q. Gu, Z. Liu and Z. Guo, *J. Mater. Chem. A*, 2015, **3**, 11930-11939.
6. X. Jiang, Y. Sha, R. Cai and Z. Shao, *J. Mater. Chem. A*, 2015, **3**, 10536-10544.
7. H.-J. Noh, S. Youn, C. S. Yoon and Y.-K. Sun, *Journal of Power Sources*, 2013, **233**, 121-130.
8. Y. K. Sun, Z. Chen, H. J. Noh, D. J. Lee, H. G. Jung, Y. Ren, S. Wang, C. S. Yoon, S. T. Myung and K. Amine, *Nature materials*, 2012, **11**, 942-947.
9. L. Zhang, N. Li, B. Wu, H. Xu, L. Wang, X. Q. Yang and F. Wu, *Nano Lett*, 2015, **15**, 656-661.
10. F. Wu, N. Li, Y. Su, L. Zhang, L. Bao, J. Wang, L. Chen, Y. Zheng, L. Dai, J. Peng and S. Chen, *Nano Lett*, 2014, **14**, 3550-3555.
11. Y. K. Sun, S. T. Myung, M. H. Kim, J. Prakash and K. Amine, *Journal of the American Chemical Society*, 2005, **127**, 13411-13418.

12. H.-H. Sun, W. Choi, J. K. Lee, I.-H. Oh and H.-G. Jung, *Journal of Power Sources*, 2015, **275**, 877-883.
13. V. Augustyn, S. Therese, T. C. Turner and A. Manthiram, *J. Mater. Chem. A*, 2015, **3**, 16604-16612.
14. A. R. Armstrong, N. Dupre, A. J. Paterson, C. P. Grey and P. G. Bruce, *Chemistry of Materials*, 2004, **16**, 3106-3118.
15. A. R. Armstrong, M. Holzapfel, P. Novak, C. S. Johnson, S. H. Kang, M. M. Thackeray and P. G. Bruce, *Journal of the American Chemical Society*, 2006, **128**, 8694-8698.
16. D. Mohanty, J. Li, D. P. Abraham, A. Huq, E. A. Payzant, D. L. Wood and C. Daniel, *Chemistry of Materials*, 2014, **26**, 6272-6280.
17. Y. Cho, P. Oh and J. Cho, *Nano Lett*, 2013, **13**, 1145-1152.
18. J. Xu, Y. Hu, T. liu and X. Wu, *Nano Energy*, 2014, **5**, 67-73.
19. N.-S. Choi, J.-G. Han, S.-Y. Ha, I. Park and C.-K. Back, *RSC Adv.*, 2015, **5**, 2732-2748.
20. J. Lu, Q. Peng, W. Wang, C. Nan, L. Li and Y. Li, *Journal of the American Chemical Society*, 2013, **135**, 1649-1652.
21. Y. K. Sun, M. J. Lee, C. S. Yoon, J. Hassoun, K. Amine and B. Scrosati, *Adv Mater*, 2012, **24**, 1192-1196.
22. C. Li, H. P. Zhang, L. J. Fu, H. Liu, Y. P. Wu, E. Ram, R. Holze and H. Q. Wu, *Electrochimica Acta*, 2006, **51**, 3872-3883.
23. K. X. Wang, X. H. Li and J. S. Chen, *Adv Mater*, 2015, **27**, 527-545.
24. R. Guo, P. Shi, X. Cheng and L. Sun, *Electrochimica Acta*, 2009, **54**, 5796-5803.
25. Z. Zheng, Z.-G. Wu, Y.-J. Zhong, C.-H. Shen, W.-B. Hua, B.-B. Xu, C. Yu, B.-H. Zhong and X.-D. Guo, *RSC Adv.*, 2015, **5**, 37330-37339.
26. P. Hou, X. Wang, D. Wang, D. Song, X. Shi, L. Zhang, J. Guo and J. Zhang, *RSC Advances*, 2014, **4**, 15923.
27. Q. Xie, Z. Hu, C. Zhao, S. Zhang and K. Liu, *RSC Adv.*, 2015, **5**, 50859-50864.
28. W. Cho, S.-M. Kim, J. H. Song, T. Yim, S.-G. Woo, K.-W. Lee, J.-S. Kim and Y.-J. Kim, *Journal of Power Sources*, 2015, **282**, 45-50.
29. F. Wu, J. Tian, Y. Su, J. Wang, C. Zhang, L. Bao, T. He, J. Li and S. Chen, *ACS applied materials & interfaces*, 2015, **7**, 7702-7708.
30. C. Zhang, P. Hou, X. Shi, D. Song, J. Song and L. Zhang, *RSC Adv.*, 2015, **5**, 36015-36021.
31. W.-H. Ryu, D.-H. Kim, S.-H. Kang and H.-S. Kwon, *RSC Advances*, 2013, **3**, 8527.
32. C.-C. Wang, Y.-C. Lin and P.-H. Chou, *RSC Adv.*, 2015, **5**, 68919-68928.
33. E.-J. Lee, H.-J. Noh, C. S. Yoon and Y.-K. Sun, *Journal of Power Sources*, 2015, **273**, 663-669.
34. K. Du, C. Hua, C. Tan, Z. Peng, Y. Cao and G. Hu, *Journal of Power Sources*, 2014, **263**, 203-208.
35. C. Gong, W. Lv, L. Qu, O. E. Bankole, G. Li, R. Zhang, M. Hu and L. Lei, *Journal of Power Sources*, 2014, **247**, 151-155.
36. W. Hua, J. Zhang, Z. Zheng, W. Liu, X. Peng, X. D. Guo, B. Zhong, Y. J. Wang and X. Wang, *Dalton transactions*, 2014, **43**, 14824-14832.
37. E. Han, Q. Jing, L. Zhu, G. Zhang and S. Ma, *Journal of Alloys and Compounds*, 2015, **618**, 629-634.
38. W. He, D. Yuan, J. Qian, X. Ai, H. Yang and Y. Cao, *Journal of Materials Chemistry A*, 2013, **1**, 11397.
39. J.-H. Park, J.-H. Cho, S.-B. Kim, W.-S. Kim, S.-Y. Lee and S.-Y. Lee, *Journal of Materials Chemistry*, 2012, **22**, 12574.
40. H. Liu, C. Chen, C. Du, X. He, G. Yin, B. Song, P. Zuo, X. Cheng, Y. Ma and Y. Gao, *J. Mater. Chem.*

- A, 2015, **3**, 2634-2641.
41. X. Li, H. Xin, Y. Liu, D. Li, X. Yuan and X. Qin, *RSC Adv.*, 2015, **5**, 45351-45358.
42. Y. Huang, X. Hou, S. Ma, X. Zou, Y. Wu, S. Hu, Z. Shao and X. Liu, *RSC Adv.*, 2015, **5**, 25258-25265.
43. B. R. Long, J. R. Croy, F. Dogan, M. R. Suichomel, B. Key, J. Wen, D. J. Miller, M. M. Thackeray and M. Balasubramanian, *Chemistry of Materials*, 2014, **26**, 3565-3572.
44. H. Yu and H. Zhou, *The Journal of Physical Chemistry Letters*, 2013, **4**, 1268-1280.
45. Y. K. Sun, S. T. Myung, B. C. Park, J. Prakash, I. Belharouak and K. Amine, *Nature materials*, 2009, **8**, 320-324.
46. Q.-F. Dong, C. Yang, Q. Zhang, W. Ding, J. Zang, M. Lei and M.-s. Zheng, *J. Mater. Chem. A*, 2015, DOI: 10.1039/c5ta00009b.
47. W. Li, J. Reimers and J. Dahn, *Physical Review B*, 1992, **46**, 3236-3246.

Figures Captions

- Figure 1.** X-ray powder diffraction patterns of the pristine and the surface modified samples. Sample S4' is the S4 after 100 charge-discharge cycles.
- Figure 2.** SEM images of the pristine and surface modified samples.
- Figure 3.** TEM images and electron diffraction patterns of the rod-like particles of sample S4.
- Figure 4.** TEM images and electron diffraction patterns of the samples S0 and S4.
- Figure 5.** (a) HAADF-STEM image and (b) STEM-EDS for (Ni, CO and Mn) and STEM-EELS for (Li), intensity line profiles extracted from the spectrum image data along the red line drawn on (a).
- Figure 6.** (a) The initial charge–discharge profiles at 27 mA g^{-1} , (b) cycle performances between 2 and 4.8V at 546 mA g^{-1} , and (c) Rate capability performances between 2 and 4.8V at difference current densities. All the electrochemical measurement were carried out at room temperature. *Here, I $C = 273 \text{ mAh g}^{-1}$.*
- Figure 7.** Cyclic voltammograms of coated and pristine LiMO_2 half-cells at a sweep rate of 0.5 mV s^{-1} in the range of 4.5 ~ 2 V at room temperature.
- Figure 8.** Nyquist plots and the equivalent circuit of the half-cells after the 1st cycle. The inset is the Nyquist plots of the cells after 100 charge-discharge cycles at 2 C.
- Figure 9.** TEM images and electron diffraction patterns of the S4 material after 100 charge-discharge cycles.

Table 1. Chemical composition of the samples.

Sample No.	Observed molar ratio	Proposed molar ratio
S0	$\text{Li}_{1.18}\text{Ni}_{0.62}\text{Co}_{0.155}\text{Mn}_{0.31}$	$\text{Li}_{1.2}\text{Ni}_{0.62}\text{Co}_{0.14}\text{Mn}_{0.24}$
S1	$\text{Li}_{1.19}\text{Ni}_{0.62}\text{Co}_{0.157}\text{Mn}_{0.322}$	$\text{Li}_{1.2}\text{Ni}_{0.62}\text{Co}_{0.14}\text{Mn}_{0.248}$
S2	$\text{Li}_{1.118}\text{Na}_{0.046}\text{Ni}_{0.62}\text{Co}_{0.157}\text{Mn}_{0.322}$	$\text{Li}_{1.15}\text{Na}_{0.05}\text{Ni}_{0.62}\text{Co}_{0.14}\text{Mn}_{0.248}$
S3	$\text{Li}_{1.115}\text{Na}_{0.077}\text{Ni}_{0.62}\text{Co}_{0.155}\text{Mn}_{0.322}$	$\text{Li}_{1.12}\text{Na}_{0.08}\text{Ni}_{0.62}\text{Co}_{0.14}\text{Mn}_{0.248}$
S4	$\text{Li}_{1.09}\text{Na}_{0.098}\text{Ni}_{0.62}\text{Co}_{0.155}\text{Mn}_{0.322}$	$\text{Li}_{1.1}\text{Na}_{0.1}\text{Ni}_{0.62}\text{Co}_{0.14}\text{Mn}_{0.248}$
S5	$\text{Li}_{1.108}\text{Na}_{0.107}\text{Ni}_{0.62}\text{Co}_{0.156}\text{Mn}_{0.321}$	$\text{Li}_{1.08}\text{Na}_{0.12}\text{Ni}_{0.62}\text{Co}_{0.14}\text{Mn}_{0.248}$

Table 2. Lattice parameters and intensity ratios of indicating peaks that calculated from XRD data.

Sample No.	a (Å)	c (Å)	c/a	I_{003}/I_{104}	Particle size (nm)*
S0	2.862	14.270	4.989	1.259	300-500
S1	2.863	14.270	4.984	1.284	200-300
S2	2.875	14.292	4.971	1.396	80-200
S3	2.890	14.300	4.948	1.595	80-200
S4	2.896	14.320	4.944	1.620	80-200
S5	2.898	14.342	4.948	1.621	80-200

*Particle size of the surface modified and the pristine materials evaluated by SEM.

Table 3. Fitting values of R_s and R_{ct} of the pristine and the surface modified materials at different state of cycling.

Cycling state	R_s and $R_{ct}(\Omega)$	S0	S1	S2	S3	S4	S5
1 st cycle	R_s	6.552	6.680	3.276	3.124	3.008	3.012
	R_{ct}	124.9	150.1	89.28	72.93	64.89	69.35
100 th cycle	R_s	8.9	6.762	3.298	3.1354	3.400	3.981
	R_{ct}	560.8	151.1	91.09	75.16	67.89	75.31

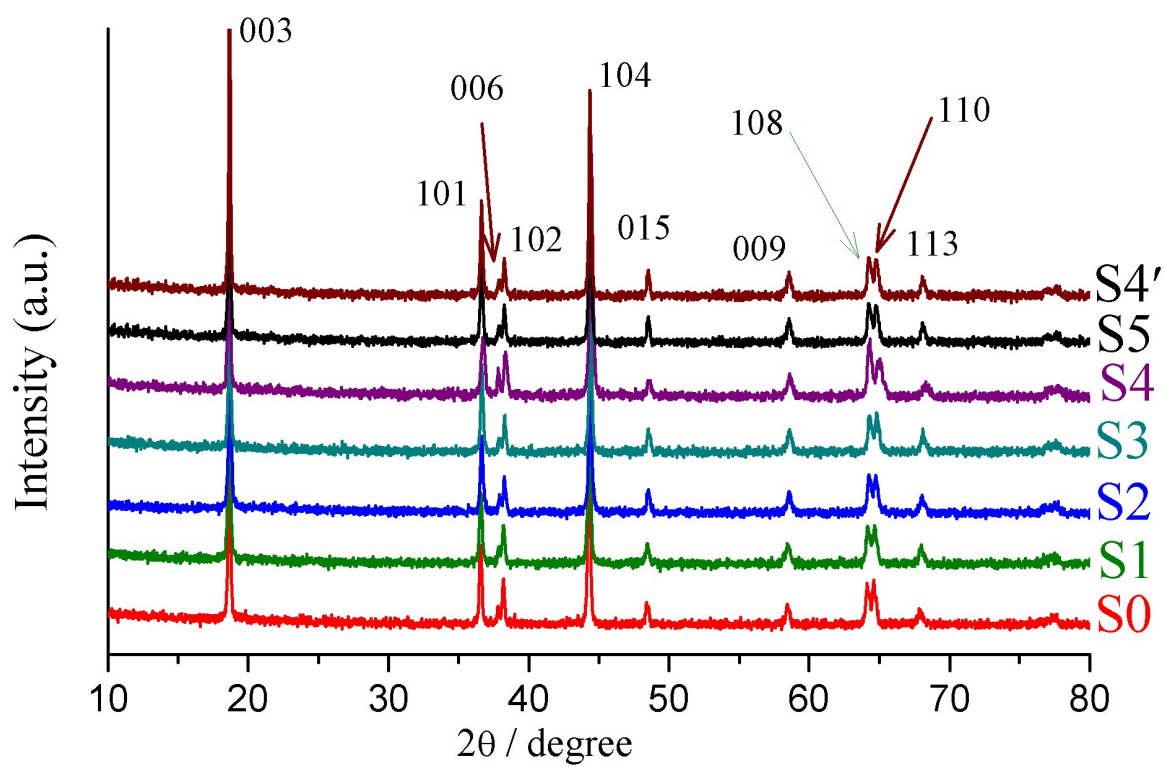


Figure 1.

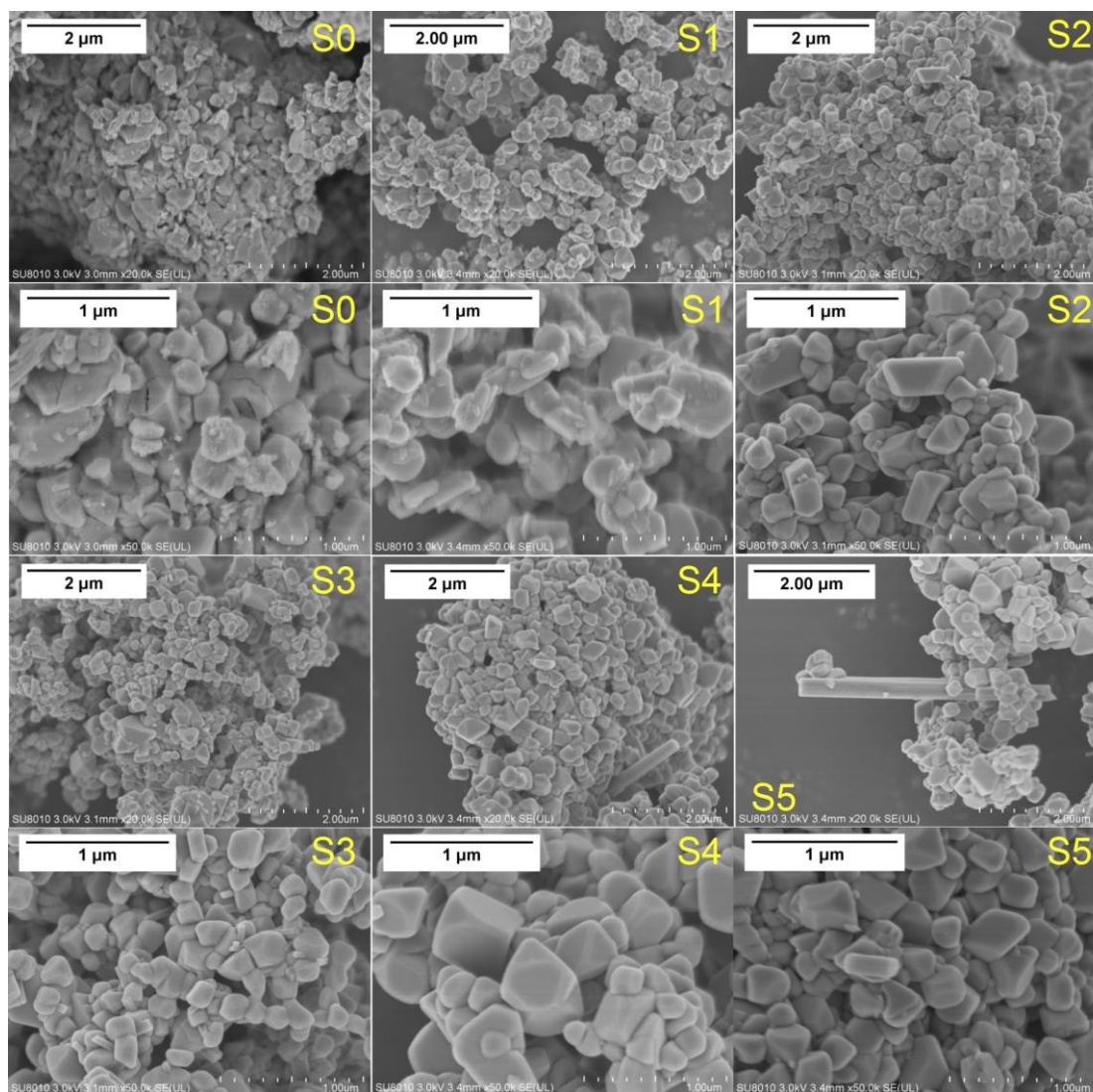


Figure 2.

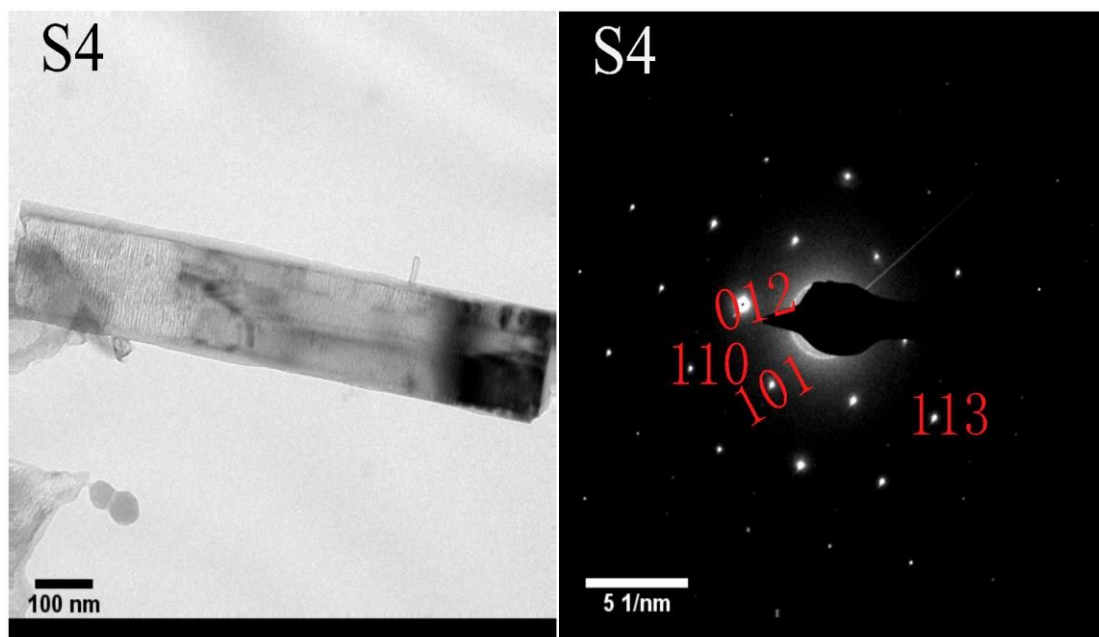


Figure 3.

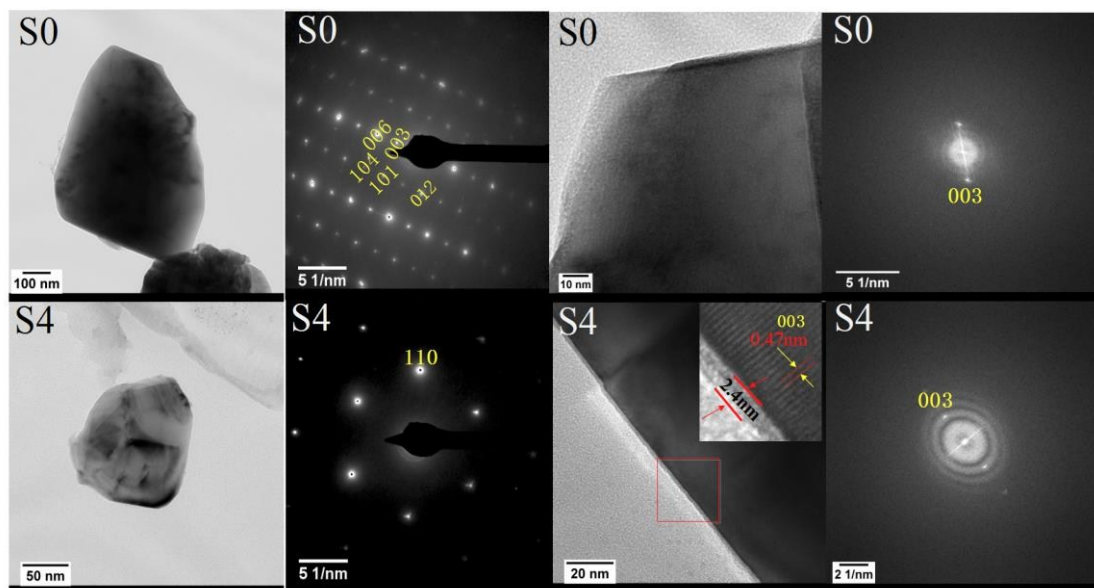


Figure 4.

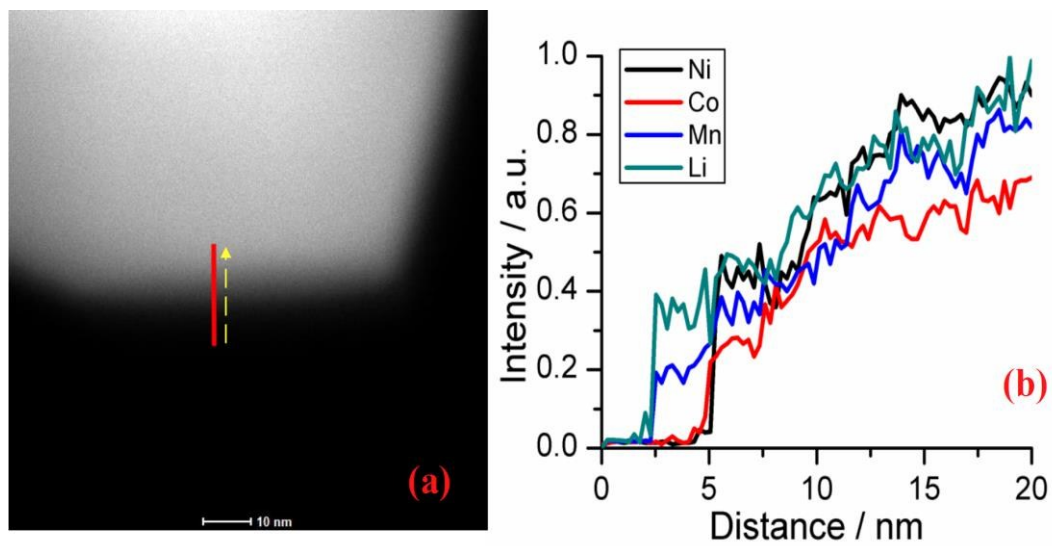


Figure 5.

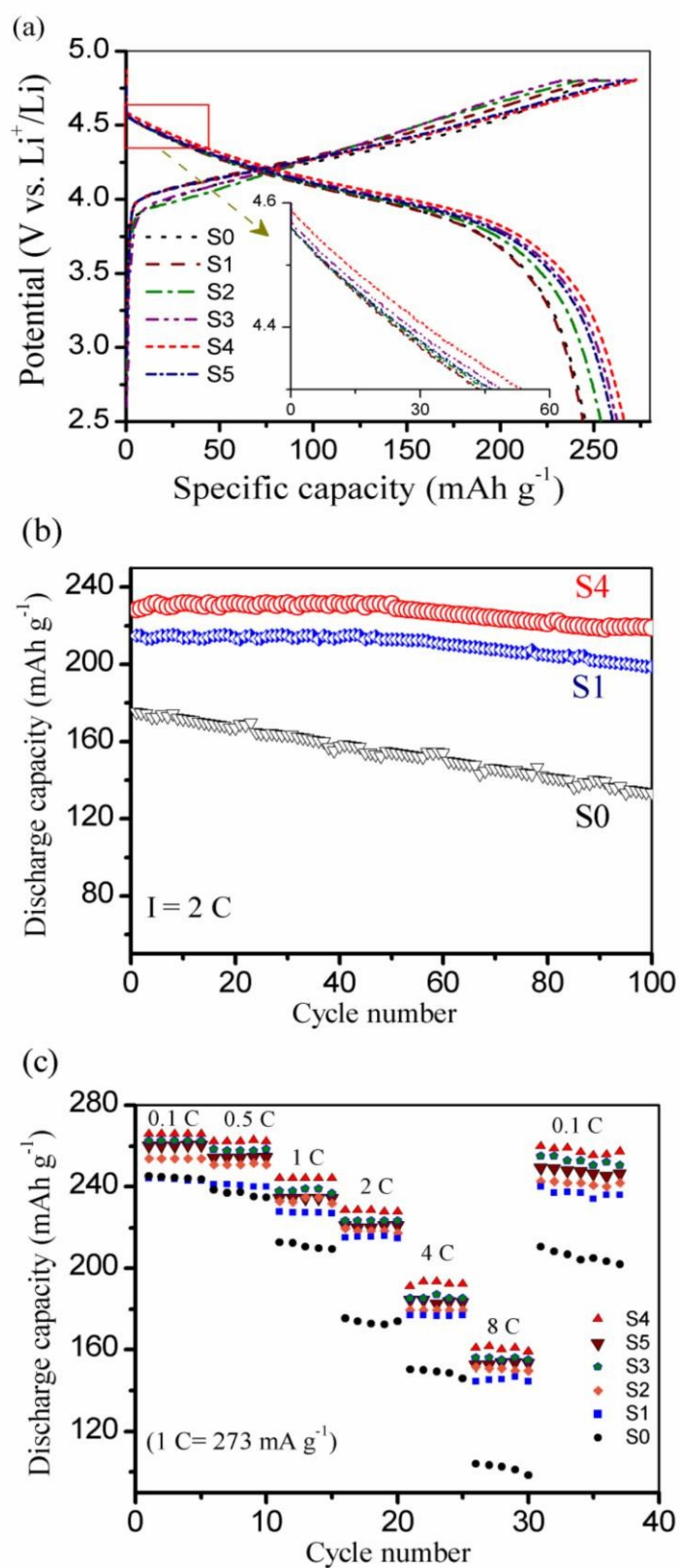


Figure 6.

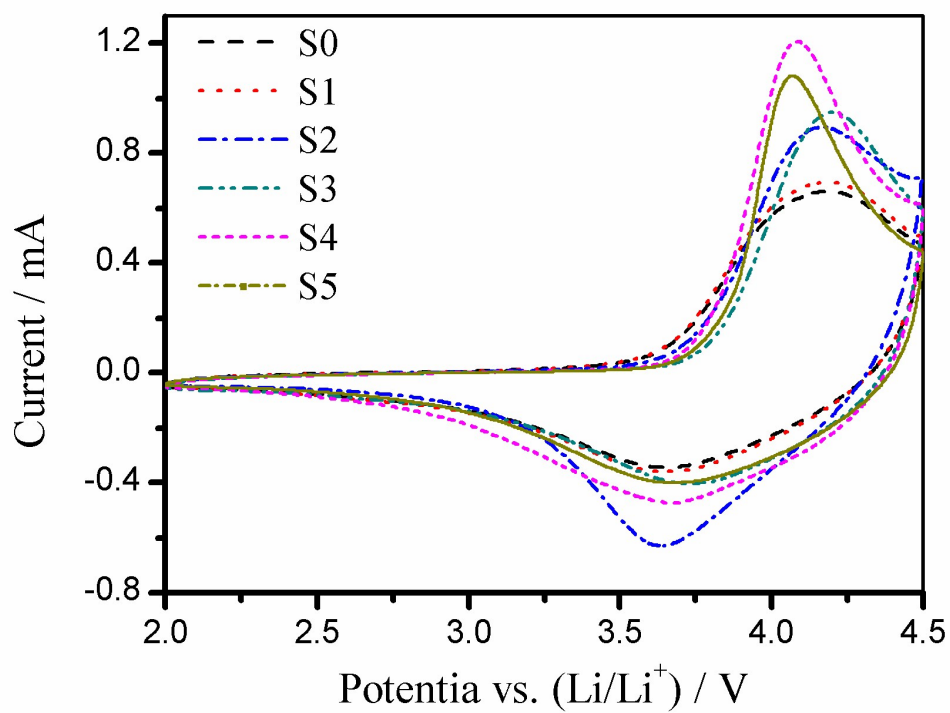


Figure 7.

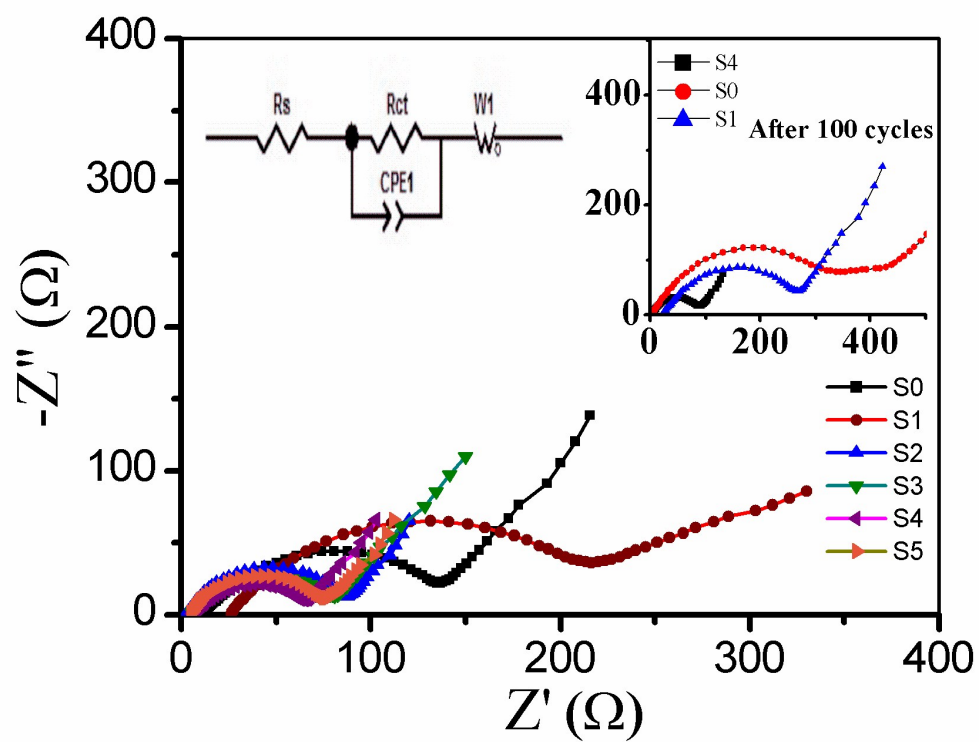


Figure 8.

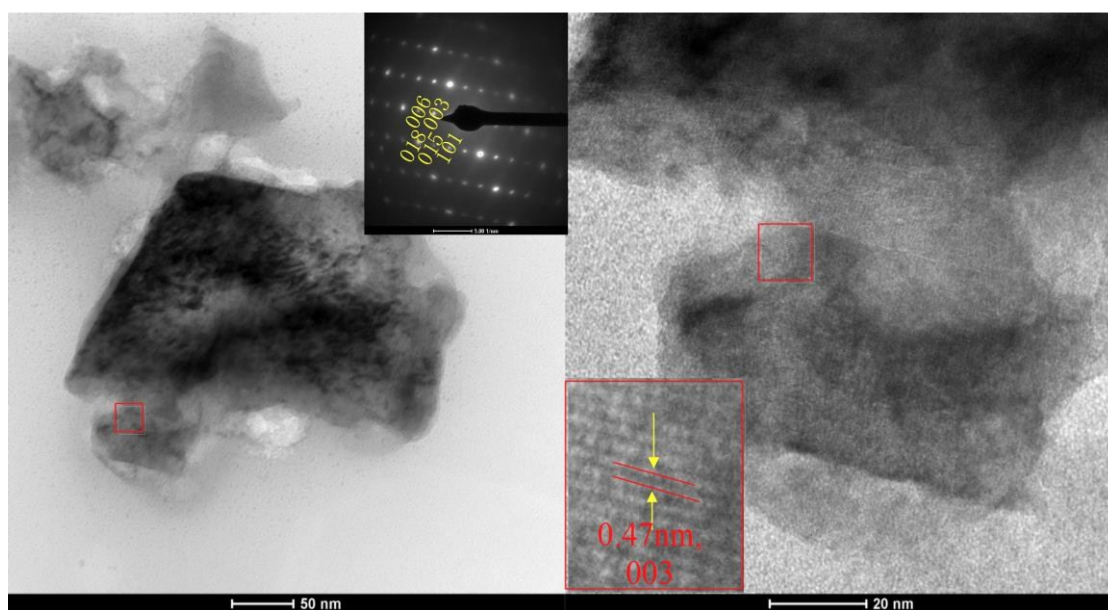
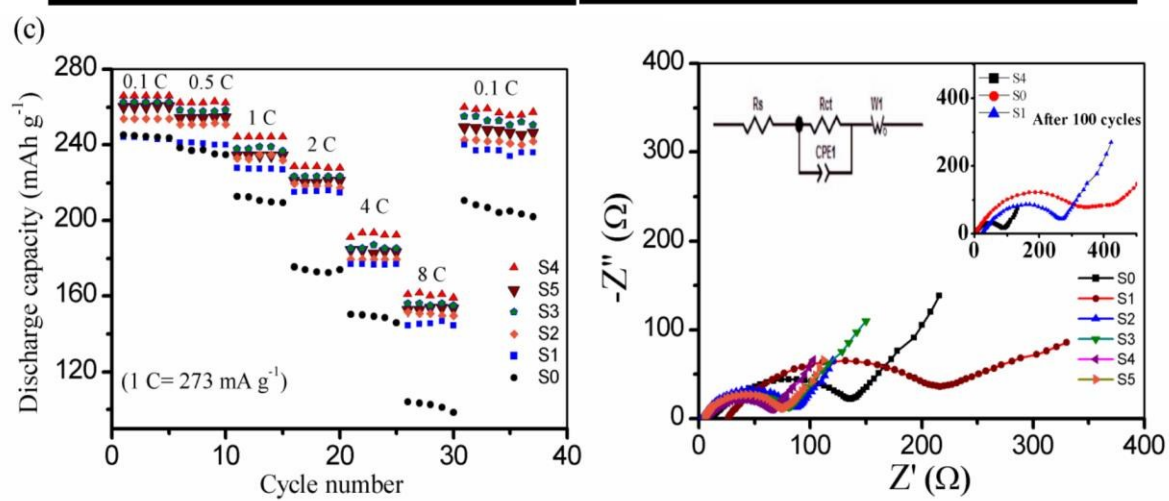
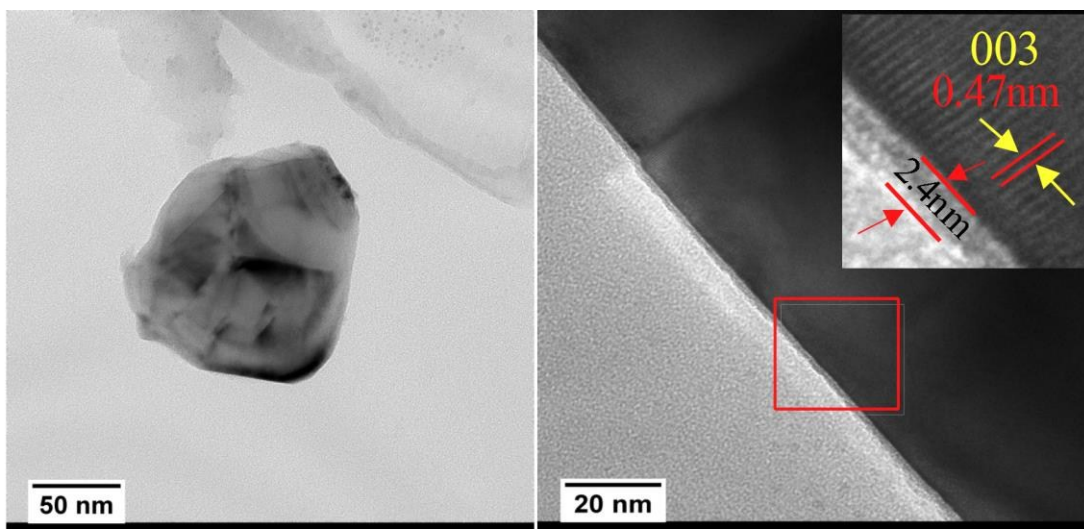


Figure 9.



Graphical Abstract